Sampled Memory-Event-Triggered Fuzzy Load Frequency Control for Wind Power Systems Subject to Outliers and Transmission Delays

Shen Yan, Zhou Gu, *Member, IEEE*, Ju H. Park, *Senior Member, IEEE*, and Xiangpeng Xie, *Member, IEEE*

***Abstract*—This study is devoted to event-triggered fuzzy load frequency control (LFC) for wind power systems (WPSs) with measurement outliers and transmission delays. Due to the integration of wind turbine (WT) with nonlinearity, the T–S fuzzy model of WPS is established for stability analysis and controller design. To mitigate the network burden, a new sampled memory-event-triggered mechanism (SMETM) related to historical system information is presented. It has the following two merits: 1) the utilization of continuous memory outputs over a given interval is useful to reduce the information loss in the period of samples and the redundant triggering events induced by disturbances and noises and 2) an extra upper constraint is added in the triggering condition to generate a new event only when the error signal belongs to a bounded range, thus, the false events caused by measurement outliers can be differentiated out and then be dropped. By representing the memory signal with transmission delay as a time-varying distributed delay term, a T–S fuzzy time-varying distributed delay system is built up to model the H_∞ LFC WPS. With the help of the Lyapunov method and the integral inequality relying on distributed delay, some criteria are derived to solve the triggering matrix and fuzzy controllers. Finally, the merits of the proposed SMETM are tested by simulation results.**

***Index Terms*—Load frequency control (LFC), measurement outliers, sampled memory-event-triggered control, wind power systems (WPSs).**

Manuscript received 29 June 2022; revised 6 October 2022; accepted 21 November 2022. Date of publication 7 December 2022; date of current version 17 May 2023. This work was supported in part by the National Natural Science Foundation of China under Grant 62103193, Grant 62273183, and Grant 62022044; in part by the Natural Science Foundation of Jiangsu Province of China under Grant BK20200769; in part by the Natural Science Foundation of Jiangsu Provincial Universities under Grant 20KJB510045; and in part by the Project funded by China Postdoctoral Science Foundation under Grant 2021TQ0155 and Grant 2022M711646. The work of Ju H. Park was supported by the National Research Foundation of Korea (NRF) Grant funded by the Korea Government (Ministry of Science and Information and Communications Technology) under Grant 2019R1A5A8080290. This article was recommended by Associate Editor C.-Y. Su. *(Corresponding authors: Zhou Gu; Ju H. Park.)*

Shen Yan and Zhou Gu are with the College of Mechanical and Electronic Engineering, Nanjing Forestry University, Nanjing 210037, China (e-mail: yanshenzdh@gmail.com; gzh1808@163.com).

Ju H. Park is with the Department of Electrical Engineering, Yeungnam University, Gyeongsan 38541, South Korea (e-mail: jessie@ynu.ac.kr).

Xiangpeng Xie is with the Institute of Advanced Technology, Nanjing University of Posts and Telecommunications, Nanjing 210023, China (e-mail: xiexp@njupt.edu.cn).

Color versions of one or more figures in this article are available at https://doi.org/10.1109/TCYB.2022.3224386.

Digital Object Identifier 10.1109/TCYB.2022.3224386

I. Introduction

Nowadays, with the expansion of population and the progress of industrialization, human demand for energy has reached a very high level. Apparently, the large consumption of fossil fuels will lead to the depletion of limited resource and the degradation of the environment. In order to mitigate this situation, some renewable and clean energy resources, such as wind energy and solar energy, have been the alternative of fossil fuels [1], [2], [3]. Compared with other energies, wind energy has the advantages like higher efficient and cost-effective, the installation areas of which can be off-shore and on-shore. Recently, the integration of wind energy and power grid becomes popular and has been used widely [4], [5], [6].

In general, there are two main types of generators in wind turbines (WTs), one is the permanent magnet synchronous generator (PMSG) and the other is the doubly fed induction generator (DFIG). In terms of the literature survey, the DFIG-based WTs have been utilized widely in the market owing to the high reliability and the effectiveness of controlling power factor, decreasing the power oscillations. As powerful tools to represent complex nonlinear dynamics, the T–S fuzzy modeling approach and the neural networks modeling approach have attracted much researchers' attention, and many valuable results can be found in [7], [8], [9], [10], [11], and [12]. To describe the nonlinear dynamical characteristics of DFIG-based WTs, the T–S fuzzy method is applied and various outcomes can be found in [13] and [14]. On the other hand, the changes of power requirement will cause the frequency of electrical power deviates from the nominal values, which could result in the damages of devices connected in the grid. For the sake of keeping the frequency stable, load frequency control (LFC) has been recognized as an effective control strategy [15], [16], [17]. As the development of network technique, the components of power systems are connected via communication networks. The networked control problems for power systems with communication delays are investigated intensively and various effective control strategies have been presented in [18], [19], and [20]. To be specific, some improved delay-dependent conditions for networked power systems with interval communication delays are obtained in [19] by applying the Bessel–Legendre inequality. In [20], the probability density of stochastic communication delay is considered to obtain some less conservative stability and controller design conditions for networked power systems. Meanwhile, the secure problem is vital for networked power systems. When the communication channels are attacked by hackers, the control performance, even stability, will be degraded. For example, a nuclear power station of Iranian was attacked by StuxNet virus, which resulted in the power failures to 60% users [21]. In a real communication network, large data transmissions generated by the time-triggered scheme may lead to the degradation of the quality of service, which could deteriorate the system stability.

In recent years, the event-triggered mechanism (ETM) has been preferred to be the alternative of the traditional time-triggered scheme. By constructing an appropriate triggering condition, only "necessary" data is triggered by ETM to control the system and the rest data, called "unnecessary," will be dropped to save the limited network resources [23], [24], [25], [26], [27], [28]. Due to this advantage, a lot of research studying the event-triggered control problems for power systems are reported in [29], [30], [31], [32], and [33] and references therein. To name a few, an adaptive ETM is used in [29] to regulate the frequency of power system. Saxena and Fridman [30] studied the LFC issue of power systems considering transmission delays by using a switching ETM. For wind power systems (WPSs) with dual denial-of-service attacks, a new method of an observed-based fault detection filter is designed in [32] to detect the cyber-attacks under a dynamic ETM. When the environment changes abruptly or unknown disturbances like strong winds or extreme cold weather happen suddenly, the sensors in practical WPSs are easy to generate measurement outliers. Compared with normal data, measurement outliers are with two distinctive features of occasional occurrences and unexpected large amplitudes. If the measurement outliers are not handled appropriately, they are inevitable to lead to false triggering events under the above ETMs [30], [31], [32], [33] and degrade the frequency stability of WPSs. In [34], a saturation-dependent strategy is proposed to reduce the negative effect of outliers on the state estimation. By taking the saturation-dependent way to suppress the measurement outliers, a fuzzy observer is designed for uncertain nonlinear systems in [35]. In fact, compared with the saturation-dependent strategy, discarding the measurement outliers directly seems a better choice. Based on this idea, an outlier-resistant ETM is investigated in [36] to distinguish the outliers and abandon them. Additionally, there usually exist stochastic and frequent fluctuations resulted from external disturbances and noises in real WPSs. There are two shortages of existing ETMs related to the instant sampled outputs in [30], [32], [33], and [36]. The one is that the some important information between two samplings may be dropped, which could degrade the control performance. The other is that these ETMs are sensitive to such stochastic fluctuations and tremendous unnecessary data will be triggered. Therefore, how to deal with the above problems motivates the current work.

According to the above analysis, this article investigates the sampled memory-event-triggered LFC issue of WPSs against measurement outliers and transmission delays. The main contributions are provided as follows.

1) *A new sampled memory-ETM (SMETM)* adopting the sampled memory signal containing historical system outputs is proposed. With the utilization of memory signal, the information loss in the intersample period is avoided and the unnecessary events induced by stochastic fluctuations can be further reduced. Moreover, an upper bound is introduced in the SMETM to restrict the triggering error signal, which is used to discard the measurement outliers and remove the false events.
2) *A united model, the time-varying distributed delay T–S fuzzy system*, is established for event-triggered LFC of WPS. In this model, the triggered memory signal with transmission delay is described by a time-varying distributed delay term. The developed united model is able to analyze the impacts of SMETM, measurement outliers, and transmission delays.
3) *A less conservative co-design strategy* is presented to design the fuzzy controller gains and the triggering matrix by applying a Lyapunov–Krasovskii functional (LKF) and an integral inequality both involved the memory signal. In contrast to Simpson's rule to treat the time-varying distributed delay in [37] and [38], there is no approximation error introduced by our strategy, which is the potential to decrease the design conservatism.

This article is organized as follows. Section II presents the preliminaries of modeling the event-triggered LFC power system with communication delays and measurement outliers. In Section III, the stability analysis and control synthesis conditions are provided. Then, the merits of the developed strategy are illustrated by some simulations in Section IV. Section V summarizes the conclusions and proposes some future investigations.

Notation: $\Im(A_1, A_2)$ equals to $A_2^T A_1 A_2$, where $A_2^\top$ means the transpose of A_2. $\otimes$ and $He(A_3)$ stand for the Kronecker product and $A_3^\top + A_3$, respectively. $\cup_{l=0}^{q}\Upsilon_l$ denotes the union of sets $\{\Upsilon_0, \dots, \Upsilon_l, \dots, \Upsilon_q\}$.

II. System Formulation

In this article, the block diagram of WPSs is shown in Fig. 1, wherein an SMETM is used to implement the LFC scheme.

A. Model of Power System

Following [22], [30], and [31], this work investigates a standard single-area power system. Let $f(t)$, $P_g(t)$, $P_t(t)$, $P_d(t)$, $ACE(t)$, and ϕ represent the frequency deviation, valve position, mechanical output of turbine, load disturbance, area control error signal, and frequency bias constant, respectively. It is common that there exist some nonlinearities in practical LFC power systems. Since the load of power system is very small when it is running at the nominal point, the linearized model can be obtained by the small signal analysis method to represent the system near the normal operating point [39], [40]. Resorting to this method, the system dynamics are linearized

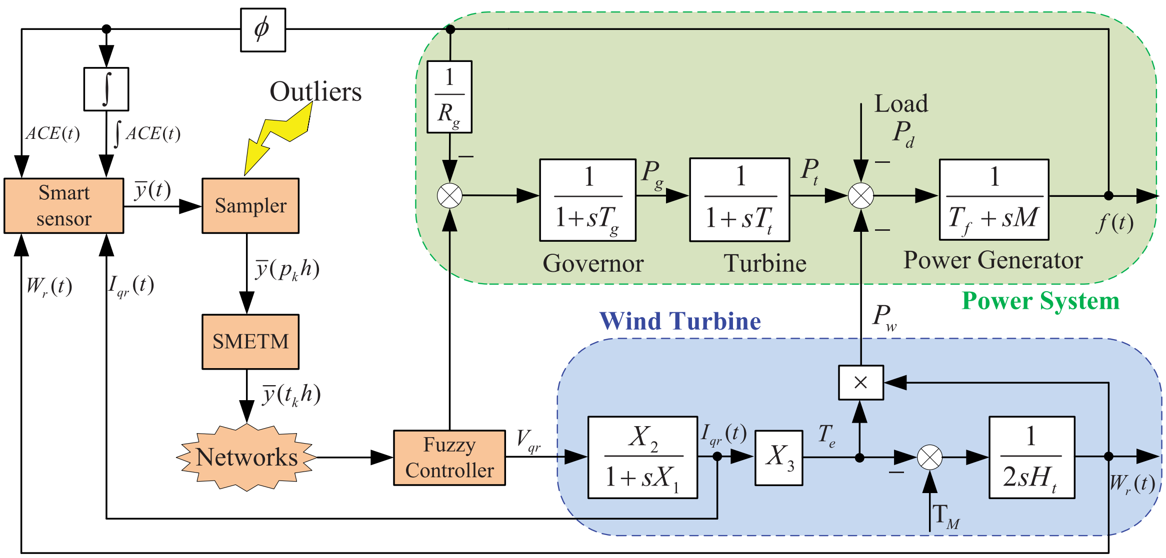

Fig. 1. Diagram of event-triggered LFC of WPS.

and represented by the next differential equations

$$\begin{cases} \dot{f}(t) = \frac{1}{M}\left(P_t(t) - P_d(t) - T_f f(t)\right) \\ \dot{P}_g(t) = \frac{1}{T_g}\left(u_f(t) - \frac{1}{R_g} f(t) - P_g(t)\right) \\ \dot{P}_t(t) = \frac{1}{T_t}\left(P_g(t) - P_t(t)\right) \\ \text{ACE}(t) = \phi f(t) \\ \int_0^t \text{ACE}(\theta)d\theta = \phi \int_0^t f(\theta)d\theta. \end{cases} \tag{1}$$

B. Model of DFIG-Based WT

It is seen that the DFIG-based WTs are trustworthy in the LFC problem and effectively utilized in the market. Here, the same DFIG-based WT model borrowed from [41] is considered as

$$\begin{cases} \dot{I}_{qr}(t) = -\frac{1}{X_1} I_{qr}(t) + \frac{X_2}{X_1} V_{qr}(t) \\ \dot{W}_r(t) = -\frac{X_3}{2H_t} I_{qr}(t) + \frac{1}{2H_t}\mathbf{T}_M(t) - B_w W_r(t) \\ P_w(t) = W_r(t) X_3 I_{qr}(t) \end{cases} \tag{2}$$

where $I_{qr}(t)$ and $V_{qr}(t)$ represent the q-axis component of the rotor current and rotor voltage, $W_r(t)$ stands for the rotational speed deviation of WT, $P_w(t)$ is the output power from WT, and B_w and H_t denote the viscous friction and inertial coefficients, respectively. And $X_1 = (\mathbb{L}_0/w_s\mathbb{R}_s)$, $\mathbb{L}_0 = (\mathbb{L}_{rr} + \mathbb{L}_m^2/\mathbb{L}_{ss})$, $\mathbb{L}_{rr} = \mathbb{L}_r + \mathbb{L}_m$, $\mathbb{L}_{ss} = \mathbb{L}_s + \mathbb{L}_m$, $X_2 = 1/\mathbb{R}_r$, and $X_3 = \mathbb{L}_m/\mathbb{L}_{ss}$ with synchronous speed w_s, stator resistance $\mathbb{R}_s$ and leakage inductance $\mathbb{L}_s$, rotor resistance $\mathbb{R}_r$ and leakage inductance $\mathbb{L}_r$, and magnetizing inductance $\mathbb{L}_m$. The mechanical power is derived from

$$\begin{aligned} \mathbf{T}_M(t) &= \frac{0.5\varrho\pi \mathbf{R}^5 \mathbf{C}_P(\beta_{opt}, \alpha) W_r^2(t)}{\beta_{opt}^3} \\ \mathbf{C}_P(\beta_{opt}, \alpha) &= (0.44 - 0.0167\alpha) \\ &\quad \times \sin\left(\frac{\pi(\beta_{opt} - 0.2)}{13 - 0.3\alpha} - 0.00184(\beta_{opt} - 2)\alpha\right) \end{aligned} \tag{3}$$

where α and β_{opt} represent the pitch angle and tip speed ratio, respectively.

C. T–S Fuzzy Model of WPS

Now, the overall system that expresses the dynamical characteristics of DFIG-based WPS is obtained as

$$\begin{cases} \dot{f}(t) = \frac{1}{M}\left(P_t(t) - P_d(t) - T_f f(t)\right. \\ \left. -W_r(t) X_3 I_{qr}(t) + W_r(t)\right) \\ \dot{P}_g(t) = \frac{1}{T_g}\left(u_f(t) - \frac{1}{R_g} f(t) - P_g(t)\right) \\ \dot{P}_t(t) = \frac{1}{T_t}\left(P_g(t) - P_t(t)\right) \\ \text{ACE}(t) = \phi f(t) \\ \dot{I}_{qr}(t) = -\frac{1}{X_1} I_{qr}(t) + \frac{X_2}{X_1} V_{qr}(t) \\ \dot{W}_r(t) = -\frac{X_3}{2H_t} I_{qr}(t) - B_w W_r(t) + \frac{1}{2H_t}\mathbf{T}_M(t). \end{cases} \tag{4}$$

By selecting the state: $x(t) = [x_1(t), x_2(t), x_3(t), x_4(t), x_5(t), x_6(t)]^\top = [f(t), P_g(t), P_t(t), \int_0^t ACE(\theta)d\theta, I_{qr}(t), W_r(t)]^\top \in \mathbb{R}^n$, system output: $y(t) = [ACE(t), \int_0^t ACE(\theta)d\theta, I_{qr}(t), W_r(t)]^\top \in \mathbb{R}^{n_y}$, control input: $u(t) = u_f(t) = V_{qr}(t)$, and disturbance: $\omega(t) = P_d(t)$, the model of WPS is formed as

$$\begin{cases} \dot{x}(t) = A(x(t))x(t) + Bu(t) + F\omega(t) \\ y(t) = Cx(t) \end{cases} \tag{5}$$

where

$$A(x(t)) = \begin{bmatrix} \frac{-T_f}{M} & 0 & \frac{1}{M} & 0 & \frac{-X_3 W_r(t)}{M} & \frac{1}{M} \\ \frac{-1}{R_g T_g} & \frac{-1}{T_g} & 0 & 0 & 0 & 0 \\ 0 & \frac{1}{T_t} & \frac{-1}{T_t} & 0 & 0 & 0 \\ \phi & 0 & 0 & 0 & 0 & 0 \\ 0 & 0 & 0 & 0 & \frac{-1}{X_1} & 0 \\ 0 & 0 & 0 & 0 & \frac{-X_3}{2H_t} & \frac{\mathbf{T}_M W_r(t)}{2H_t} - B_w \end{bmatrix}$$

$$\mathbf{T}_M = \frac{0.5\varrho\pi\mathbf{R}^5\mathbf{C}_P(\beta_{opt}, \alpha)}{\beta_{opt}^3}, B^\top = \begin{bmatrix} 0 & \frac{1}{T_g} & 0 & 0 & \frac{X_2}{X_1} & 0 \end{bmatrix}^\top$$

$$F^\top = \begin{bmatrix} -\frac{1}{M} & 0 & 0 & 0 & 0 & 0 \end{bmatrix}, \; C = \begin{bmatrix} \phi & 0 & 0 & 0 & 0 & 0 \\ 0 & 0 & 0 & 1 & 0 & 0 \\ 0 & 0 & 0 & 0 & 1 & 0 \\ 0 & 0 & 0 & 0 & 0 & 1 \end{bmatrix}.$$

In order to achieve the stability criteria of system (5), the following two rule T–S fuzzy system is considered as follows.

Plant Rule i: IF $W_r(t)$ is φ_i^s, THEN

$$\begin{cases} \dot{x}(t) = A_i x(t) + Bu(t) + F\omega(t) \\ y(t) = Cx(t) \end{cases} \tag{6}$$

where $W_r(t) \in [W_{r\min}, W_{r\max}]$ is the premise variable, $\varphi_i^s (s = 1)$ means the fuzzy set, and

$$A_1 = \begin{bmatrix} \frac{-T_f}{M} & 0 & \frac{1}{M} & 0 & \frac{-X_3 W_{r\min}}{M} & \frac{1}{M} \\ \frac{-1}{R_g T_g} & \frac{-1}{T_g} & 0 & 0 & 0 & 0 \\ 0 & \frac{1}{T_t} & \frac{-1}{T_t} & 0 & 0 & 0 \\ \phi & 0 & 0 & 0 & 0 & 0 \\ 0 & 0 & 0 & 0 & \frac{-1}{X_1} & 0 \\ 0 & 0 & 0 & 0 & \frac{-X_3}{2H_t} & \frac{\mathbf{T}_M W_{r\min}}{2H_t} - B_w \end{bmatrix}$$

$$A_2 = \begin{bmatrix} \frac{-T_f}{M} & 0 & \frac{1}{M} & 0 & \frac{-X_3 W_{r\max}}{M} & \frac{1}{M} \\ \frac{-1}{R_g T_g} & \frac{-1}{T_g} & 0 & 0 & 0 & 0 \\ 0 & \frac{1}{T_t} & \frac{-1}{T_t} & 0 & 0 & 0 \\ \phi & 0 & 0 & 0 & 0 & 0 \\ 0 & 0 & 0 & 0 & \frac{-1}{X_1} & 0 \\ 0 & 0 & 0 & 0 & \frac{-X_3}{2H_t} & \frac{\mathbf{T}_M W_{r\max}}{2H_t} - B_w \end{bmatrix}.$$

By denoting the normalized membership function $\lambda_1(t) = [1/2](1 + [W_r(t)]/[W_{r\max}])$, $\lambda_2(t) = 1 - \lambda_1(t)$, the T–S fuzzy WPS is expressed by

$$\begin{cases} \dot{x}(t) = \sum_{i=1}^{2} \lambda_i(W_r(t))\big(A_i x(t) + Bu(t) + F\omega(t)\big) \\ y(t) = Cx(t) \\ z(t) = Cx(t) \end{cases} \tag{7}$$

where $z(t) \in \mathbb{R}^{n_z}$ is the performance output, and $\lambda_i(W_r(t))$ is simplified as λ_i and satisfies

$$\sum_{i=1}^{2} \lambda_i(t) = 1, \ \ v_M(t) = \lambda_1(t) W_{r\min} + \lambda_2(t) W_{r\max}.$$

D. Sampled-Memory-Event-Triggered Mechanism

To release the network transmission burden, a new SMETM integrated with a continuous memory signal and sampling scheme is constructed to determine the next triggering time, which is given as

$$\begin{aligned} t_{k+1}h = t_k h + \min_{l}\{l > 0 | \rho_1 \Im(\Omega, \bar{y}(t_k h)) \le \Im(\Omega, \varepsilon(t)) \\ \le \rho_2 \Im(\Omega, \bar{y}(t_k h))\} \end{aligned} \tag{8}$$

where

$$\begin{aligned} &\varepsilon(t) \triangleq \bar{y}(p_k h) - \bar{y}(t_k h), \bar{y}(t) \triangleq \frac{1}{\chi} \int_{t-\chi}^{t} y(\theta) d\theta \\ &p_k h = t_k h + lh, \ \ l \in [0, t_{k+1} - t_k) \end{aligned}$$

and h is the sampling period, $t_k h$ and $t_{k+1} h$ stand for the latest and the next triggering instant, respectively; $p_k h$ denotes the current sampling time; $\Omega > 0$, $\rho_1 > 0$, and $\rho_2 > 0$ are the triggering matrix, and the lower and upper triggering thresholds; and $\chi > h > 0$ means the time interval of continuous historical outputs. By taking into account the communication delay and utilizing zero-order hold (ZOH), the input of the controller is expressed by

$$\tilde{y}(t) = \bar{y}(t_k h), \ \ t \in \Upsilon \triangleq [t_k h + \tau_k, \ \ t_{k+1} h + \tau_{k+1}) \tag{9}$$

in which $\tau_k \in [0, \ \bar{\tau}]$ means the communication delay. By defining $\Upsilon_l = [t_k h + lh + d_l, \ \ t_k h + (l+1)h + d_{l+1})$, it gives $\Upsilon = \cup_{l=0}^{t_{k+1}-t_k} \Upsilon_l$ with $d_0 = \tau_k$ and $d_{t_{k+1}-t_k} = \tau_{k+1}$. For $t \in \Upsilon_l$, a piecewise delay $\tau(t) \triangleq t - i_k h$ is defined and $0 \le \tau(t) \le \tau_M = \bar{\tau} + h$. Then, the triggered signal $\bar{y}(t_k h)$ can further formulated by

$$\bar{y}(t_k h) = \bar{y}(t - \tau(t)) - \varepsilon(t) = \frac{C}{\chi} \int_{t-\tau(t)-\chi}^{t-\tau(t)} x(s) ds - \varepsilon(t). \tag{10}$$

Remark 1: Note that some important information in the intersample period will be lost in the conventional ETMs related to current sampled data $y(p_k h)$ [23], [29]. In order to avoid such case, the sampled memory data $\bar{y}(p_k h)$ containing the continuous past outputs, instead of $y(p_k h)$, is inputted to SMETM (8).

Remark 2: Two parameters ρ_1 and ρ_2 satisfying $0 < \rho_1 < \rho_2$ are introduced in SMETM (8), where ρ_1 accounts for reducing the unnecessary signals induced by disturbances and ρ_2 is used to discard the false events resulted from the measurement outliers. When χ equals to zero, our SMETM (8) is converted to the existing outlier-resilient ETM (ORETM) in [36]. Additionally, when $\chi = 0$ and $\rho_2 \to \infty$, it further becomes the normal ETMs in [23] and [43].

Remark 3: According to (10), the continuous memory output, discrete sampling, and communication delays are combined in a united time-varying distributed delay model. Compared with the integral-based ETMs using memory signal [37], [44] without taking into account the time-varying delays, our proposed model (10) is more practical and general.

Remark 4: With the use of the memory signal $\bar{y}(t)$, the provided SMETM is the potential to reduce the releasing rate, which can be increased by high-frequency disturbances and noises. Meanwhile, the sampled scheme is able to exclude the Zeno behavior naturally.

E. Closed-Loop System of WPS

Following the similar way for obtaining system (7), the T–S fuzzy controller is designed as

$$u(t) = \sum_{j=1}^{2} \lambda_j^k K_j \bar{y}(t_k h) \tag{11}$$

where λ_j^k is the abbreviation of $\lambda_j(W_r(t_k h))$. Additionally, the same assumption $\lambda_j^k - \nu_j \lambda_j \ge 0$ with [42] is utilized in this work.

By defining $\eta(t) \triangleq \tau(t) + \chi$, $\chi \le \eta(t) \le \eta_M \triangleq \tau_M + \chi$ and rewriting $\bar{y}(t_k h)$ as

$$\bar{y}(t_k h) = \frac{C}{\chi} \left[\int_{t-\chi}^{t} x(s) ds + \int_{t-\eta(t)}^{t-\chi} x(s) ds - \int_{t-\tau(t)}^{t} x(s) ds \right] - \varepsilon(t) \tag{12}$$

it leads to the closed-loop LFC system as

$$\dot{x}(t) = \sum_{i=1}^{2}\sum_{j=1}^{2}\lambda_i\lambda_j^k\Big(A_i x(t) - BK_j\varepsilon(t) + F\omega(t) + BK_j\frac{C}{\chi}\Big[\int_{t-\chi}^{t}x(s)ds + \int_{t-\eta(t)}^{t-\chi}x(s)ds - \int_{t-\tau(t)}^{t}x(s)ds\Big]. \quad (13)$$

For the simplicity of analysis and derivation, the following abbreviations and Legendre polynomials are defined as:

$$\mathbf{e}_i \triangleq \begin{cases} \big[0_{n,n(i-1)}\ I_n\ 0_{n,n(10+5\kappa-i)+n_y+1+n_z}\big] & i = 1,\ldots,10+5\kappa \\ \big[0_{n_y,n(10+5\kappa)}\ I_{n_y}\ 0_{n_y,1+n_z}\big], & i = 11+5\kappa \\ \big[0_{1,n(10+5\kappa)+n_y}\ I_1\ 0_{1,n_z}\big], & i = 12+5\kappa \\ \big[0_{n_z,n(10+5\kappa)+n_y+1}\ I_{n_z}\big], & i = 13+5\kappa \end{cases}$$

$$\mathbb{D}_m(\theta) \triangleq \mathcal{D}_{m,\kappa}(\theta)\otimes I,\ \ m = 1,2,3,\ \ \theta \in [\theta_{m,1},\ \theta_{m,2}]$$

$$\mathcal{D}_{m,\kappa}(\theta) \triangleq \big[D_{m,0}(\theta)\cdots D_{m,r}(\theta)\cdots D_{m,\kappa}(\theta)\big]^\top$$

$$D_{m,r}(\theta) = (-1)^r\sum_{v=0}^{r}P_v^r\Big(\frac{\theta-\theta_{k,1}}{\theta_{k,2}-\theta_{k,1}}\Big)^r$$

$$P_v^r = (-1)^r\binom{r}{v}\binom{r+v}{r}$$

$$\mathscr{D}_m(t) = \int_{\theta_{m,1}}^{\theta_{m,2}}\mathbb{D}_m(\theta)x(t+\theta)d\theta$$

$$\mathfrak{D}_m(t) = \begin{bmatrix}\mathscr{D}_{m,1}(t)\\ \mathscr{D}_{m,2}(t)\end{bmatrix},\ \ m = 1,3,\ \ \mathfrak{D}_2(t) = \mathscr{D}_2(t)$$

$$\mathscr{D}_{m,1}(t) = \int_{-\vartheta_m(t)}^{\theta_{m,2}}\mathbb{D}_m(\theta)x(t+\theta)d\theta$$

$$\mathscr{D}_{m,2}(t) = \int_{\theta_{m,1}}^{-\vartheta_m(t)}\mathbb{D}_m(\theta)x(t+\theta)d\theta$$

$$\theta_{1,1} = -\tau_M,\ \ \vartheta_1(t) = \tau(t),\ \ \theta_{1,2} = 0,\ \ \theta_{2,1} = -\chi$$

$$\theta_{2,2} = 0,\ \ \theta_{3,1} = -\eta_M,\ \ \vartheta_3(t) = \eta(t),\ \ \theta_{3,2} = -\chi.$$

Based on the above definitions, system (13) is further deduced as

$$\dot{x}(t) = \sum_{i=1}^{2}\sum_{j=1}^{2}\lambda_i\lambda_j^k\Big[A_i x(t) - BK_j\varepsilon(t) + F\omega(t) + \frac{BK_jC\mathfrak{I}}{\chi}\big(\mathscr{D}_2(t) + \mathscr{D}_{1,1}(t) - \mathscr{D}_{3,1}(t)\big)\Big] \quad (14)$$

where $\mathfrak{I} = [I_n\ 0_{n,\kappa n}]$.

This article contributes to design the event-triggered fuzzy controller (11) satisfying the following.

1) For $\omega(t) = 0$, the system (14) is asymptotically stable.
2) For $\omega(t) \neq 0$ and $x(0) = 0$, the disturbance attenuation level $\gamma > 0$ is guaranteed by $\int_0^\infty z^\top(t)z(t)dt < \gamma^2\int_0^\infty \omega^\top(t)\omega(t)dt$.

Before ending this section, a technical lemma is provided as follows.

Lemma 1: For matrices $H \in \mathbb{R}^{q\times q} > 0$, $X \in \mathbb{R}^{q\times q}$, $\mathcal{H} > 0$ and a vector function $x(\theta) \in \mathbb{R}^q$, $c(\theta) \in [c_1,\ c_2]$, it gives

$$\int_{c_1}^{c_2}\Im(H, x(\theta))d\theta \geq \frac{1}{c_2 - c_1}\Im\Big(\mathcal{H}\otimes\mathfrak{R}, \begin{bmatrix}\mathbf{D} & 0_{q\kappa}\\ 0_{q\kappa} & \mathbf{D}\end{bmatrix}\Pi\Big) \quad (15)$$

where $\mathfrak{R} = \mathrm{diag}\{1, 3, \ldots, 2\kappa+1\}$

$$\mathbb{D}(\theta) \triangleq \mathcal{D}_\kappa(\theta)\otimes I_q,\ \ \mathcal{D}_\kappa(\theta) \triangleq [D_0(\theta)\cdots D_r(\theta)\cdots D_\kappa(\theta)]^\top$$

$$\mathcal{H} = \begin{bmatrix}H & X\\ X^\top & H\end{bmatrix},\ \ \Pi = \begin{bmatrix}\int_{c(\theta)}^{c_2}\mathbb{D}(\theta)x(\theta)d\theta\\ \int_{c_1}^{c(\theta)}\mathbb{D}(\theta)x(\theta)d\theta\end{bmatrix}$$

and $D_r(\theta) = (-1)^r\sum_{v=0}^{r}(-1)^v\binom{r}{v}\binom{r+v}{r}([\theta - c_1]/[c_2 - c_1])^r$ are Legendre polynomials satisfying the properties provided in [45].

Proof: The condition (15) is achieved by taking $\varpi(s) = 1$ and choosing Legendre polynomials $D_i(\theta)$ as the distributed delay kernel $\mathbf{f}(s)$ in [46, Lemma 3], and then the proof is fulfilled. ■

Remark 5: The matrix $\mathbf{D}$ denotes the communication matrix for the Kronecker product, which has the same property provided in [46, Lemma 2]. In addition, it can be obtained by solving MATLAB function **vecperm**(q, v) [47].

III. Main Results

First, the H_∞ stability analysis conditions for system (14) are deduced in Theorem 1.

Theorem 1: For given parameters $\bar{\tau}$, μ_i, a_i, v_i, $(i = 1, 2)$, under the SMETM (8) with the scalars ρ_1, ρ_2, h, χ, and the controller gains K_j, the asymptotically stability with H_∞ norm bound γ of system (14) is ensured, if there exist symmetric matrices G, $H_b > 0$, $J_b > 0$, $(b = 1, 2, 3)$, $\mathcal{J}_r = \begin{bmatrix}J_r & R_r^\top\\ R_r & J_r\end{bmatrix} > 0$, $(r = 1, 3)$, $\Omega > 0$ and matrix W such that

$$\mathscr{G} > 0 \quad (16)$$

$$\Pi_{ij} - \mho_i < 0 \quad (17)$$

$$\digamma_{ii} < 0 \quad (18)$$

$$\digamma_{ij} + \digamma_{ji} < 0,\quad (i < j) \quad (19)$$

where

$$\mathscr{G} = G + \mathrm{diag}\Big\{0, \frac{\mathscr{H}_1}{\tau_M}, \frac{\mathscr{H}_2}{\chi}, \frac{\mathscr{H}_3}{\tau_M}\Big\}$$

$$\mathscr{H}_1 = \mathfrak{R}\otimes H_1,\ \mathscr{H}_2 = \mathfrak{R}\otimes H_2,\ \mathscr{H}_3 = \mathfrak{R}\otimes H_3$$

$$\Pi_{ij} = \Theta + He(\mathbf{W}\mathbf{Q}_{ij}),\ \ \digamma_{ij} = v_j(\Pi_{ij} - \mho_i) + \mho_i$$

$$\begin{aligned}\Theta = {} & He\big(\Delta_1^{\top G}\Delta_2\big) + \Im(H_1 + \tau_M J_1 + H_2 + \chi J_2, \mathbf{e}_2) \\ & - \Im(H_1, \mathbf{e}_3) + \Im(H_3 + \tau_M J_3 - H_2, \mathbf{e}_4) - \Im(H_3, \mathbf{e}_5) \\ & - \frac{1}{\chi}\Im(\mathscr{J}_2, \mathbf{e}_b) - \frac{1}{\tau_M}\Im(\mathscr{J}_1, \mathbf{D}\mathbf{e}_a) - \frac{1}{\tau_M}\Im(\mathscr{J}_3, \mathbf{D}\mathbf{e}_c) \\ & + a_1\rho_1\Im\Big(\Omega, \frac{C\mathfrak{I}}{\chi}\mathbf{e}_\chi - \mathbf{e}_{11+5\kappa}\Big) - a_1\Im(\Omega, \mathbf{e}_{11+5\kappa}) \\ & - a_2\rho_2\Im\Big(\Omega, \frac{C\mathfrak{I}}{\chi}\mathbf{e}_\chi - \mathbf{e}_{11+5\kappa}\Big) + a_2\Im(\Omega, \mathbf{e}_{11+5\kappa}) \\ & - \gamma^2\Im(I, \mathbf{e}_{12+5\kappa}) - \Im(I, \mathbb{I}_{13+5\kappa}) + He\big(\mathbf{e}_{13+5\kappa}^\top C\mathbf{e}_2\big)\end{aligned}$$

$$\mathscr{J}_2 = \mathfrak{R}\otimes J_2,\ \mathscr{J}_1 = \mathcal{J}_1\otimes\mathfrak{R},\ \mathscr{J}_3 = \mathcal{J}_3\otimes\mathfrak{R}$$

$$\Delta_1 = \begin{bmatrix}\mathbf{e}_2\\ \mathbf{e}_{a,1} + \mathbf{e}_{a,2}\\ \mathbf{e}_b\\ \mathbf{e}_{c,1} + \mathbf{e}_{c,2}\end{bmatrix},\ \Delta_2 = \begin{bmatrix}\mathbf{e}_1\\ \mathbf{E}_1\mathbf{e}_2 - \mathbf{E}_2\mathbf{e}_3 + \frac{\Psi_\kappa}{\tau_M}(\mathbf{e}_{a,1} + \mathbf{e}_{a,2})\\ \mathbf{E}_1\mathbf{e}_2 - \mathbf{E}_2\mathbf{e}_4 + \frac{\Psi_\kappa}{\chi}\mathbf{e}_b\\ \mathbf{E}_1\mathbf{e}_5 - \mathbf{E}_2\mathbf{e}_5 + \frac{\Psi_\kappa}{\tau_M}(\mathbf{e}_{c,1} + \mathbf{e}_{c,2})\end{bmatrix}$$

$$\mathbf{e}_a = \begin{bmatrix}\mathbf{e}_{a,1}\\ \mathbf{e}_{a,2}\end{bmatrix},\ \mathbf{e}_{a,1} = \begin{bmatrix}\mathbf{e}_6\\ \vdots\\ \mathbf{e}_{6+\kappa}\end{bmatrix},\ \mathbf{e}_{a,2} = \begin{bmatrix}\mathbf{e}_{7+\kappa}\\ \vdots\\ \mathbf{e}_{7+2\kappa}\end{bmatrix}$$

$$
\begin{aligned}
&\mathbf{e}_c = \begin{bmatrix} \mathbf{e}_{c,1} \\ \mathbf{e}_{c,2} \end{bmatrix},\ \mathbf{e}_{c,1} = \begin{bmatrix} \mathbf{e}_{9+3\kappa} \\ \vdots \\ \mathbf{e}_{9+4\kappa} \end{bmatrix},\ \mathbf{e}_{c,2} = \begin{bmatrix} \mathbf{e}_{10+4\kappa} \\ \vdots \\ \mathbf{e}_{10+5\kappa} \end{bmatrix} \\
&\mathbf{e}_b = \begin{bmatrix} \mathbf{e}_{8+2\kappa} \\ \vdots \\ \mathbf{e}_{8+3\kappa} \end{bmatrix},\ \mathbf{E}_1 = \begin{bmatrix} I_n \\ \vdots \\ I_n \end{bmatrix},\ \mathbf{E}_2 = \begin{bmatrix} (-1)^0 I_n \\ \vdots \\ (-1)^\kappa I_n \end{bmatrix} \\
&\Psi_\kappa = \begin{bmatrix} \psi_0^0 I & \cdots & \psi_0^\kappa I \\ \vdots & \psi_k^i & \vdots \\ \psi_\kappa^0 I & \cdots & \psi_\kappa^\kappa I \end{bmatrix},\ \psi_k^i = \begin{cases} -(2i+1)\left(1-(-1)^{k+i}\right), & i \le k \\ 0, & i > k \end{cases} \\
&\mathbf{W} = \mu_1 \mathbf{e}_1^\top W + \mu_2 \mathbf{e}_2^\top W,\ \ \mathbf{e}_\chi = \mathbf{e}_b + \mathbf{e}_{a,1} - \mathbf{e}_{c,1} \\
&\mathbf{Q}_{ij} = -\mathbf{e}_1 + A_i \mathbf{e}_2 - BK_j \mathbf{e}_{11+5\kappa} + F\mathbf{e}_{12+5\kappa} + \frac{BK_j C\Im}{\chi}\mathbf{e}_\chi.
\end{aligned}
$$

Proof: We define $\delta^\top(t) = \left[x^\top(t), \mathscr{D}_1^\top(t), \mathscr{D}_2^\top(t), \mathscr{D}_3^\top(t)\right]^\top$ and construct an LKF as

$$
L(t) = \sum_{i=1}^{4} L_i(t) \tag{20}
$$

where

$$
\begin{aligned}
L_1(t) &= \delta^\top(t) G \delta(t) \\
L_2(t) &= \int_{t-\tau_M}^{t} \Im(H_1 + (\theta - t + \tau_M)J_1, x(\theta))d\theta \\
L_3(t) &= \int_{t-\chi}^{t} \Im(H_2 + (\theta - t + \chi)J_2, x(\theta))d\theta \\
L_4(t) &= \int_{t-\eta_M}^{t-\chi} \Im(H_3 + (\theta - t + \eta_M)J_3, x(\theta))d\theta.
\end{aligned}
$$

By applying [48, Lemma 5], it yields

$$
\int_{t-\tau_M}^{t} \Im(H_1, x(\theta))d\theta \ge \frac{1}{\tau_M}\Im(\mathscr{H}_1, \mathscr{D}_1(t)) \tag{21}
$$

$$
\int_{t-\chi}^{t} \Im(H_2, x(\theta))d\theta \ge \frac{1}{\chi}\Im(\mathscr{H}_2, \mathscr{D}_2(t)) \tag{22}
$$

$$
\int_{t-\eta_M}^{t-\chi} \Im(H_3, x(\theta))d\theta \ge \frac{1}{\tau_M}\Im(\mathscr{H}_3, \mathscr{D}_3(t)). \tag{23}
$$

In terms of $H_l > 0$, $J_l > 0$, $l = 1, 2, 3$, and $\mathscr{G} > 0$ in (16), $L(t) > 0$ is ensured.

Define

$$
\pi^\top(t) = \left[\pi_1^\top(t)\ \pi_2^\top(t)\right] \tag{24}
$$

where

$$
\begin{aligned}
\pi_1^\top(t) &= \left[\dot{x}^\top(t), x^\top(t), x^\top(t-\tau_M), x^\top(t-\chi), x^\top(t-\eta_M)\right] \\
\pi_2^\top(t) &= \left[\mathfrak{D}_1{}^\top(t), \mathfrak{D}_2{}^\top(t), \mathfrak{D}_3{}^\top(t), \varepsilon^\top(t), \varpi^\top(t), z^\top(t)\right].
\end{aligned}
$$

The time derivative of $L(t)$ is computed as

$$
\begin{aligned}
\dot{L}(t) = He&\left(\delta^\top(t) G \dot{\delta}(t)\right) \\
&+ \Im(H_1 + \tau_M J_1, x(t)) - \Im(H_1, x(t-\tau_M)) \\
&+ \Im(H_2 + \chi J_2, x(t)) - \Im(H_2, x(t-\chi)) \\
&+ \Im(H_3 + \tau_M J_3, x(t-\chi)) - \Im(H_3, x(t-\eta_M)) \\
&- \int_{-\tau_M}^{0} \Im(J_1, x(t+\theta))d\theta - \int_{-\chi}^{0} \Im(J_2, x(t+\theta))d\theta \\
&- \int_{-\eta_M}^{-\chi} \Im(J_3, x(t+\theta))d\theta.
\end{aligned} \tag{25}
$$

Recalling the bound and differentiation properties of Legendre polynomials in [45], we have

$$
\dot{\mathscr{D}}_1(t) = \mathbf{E}_1 x(t) - \mathbf{E}_2 x(t-\tau_M) + \frac{\Psi_\kappa}{\tau_M}\left(\mathscr{D}_{1,1}(t) + \mathscr{D}_{1,2}(t)\right) \tag{26}
$$

$$
\dot{\mathscr{D}}_2(t) = \mathbf{E}_1 x(t) - \mathbf{E}_2 x(t-\chi) + \frac{\Psi_\kappa}{\chi}\mathscr{D}_2(t) \tag{27}
$$

$$
\dot{\mathscr{D}}_3(t) = \mathbf{E}_1 x(t-\chi) - \mathbf{E}_2 x(t-\eta_M) + \frac{\Psi_\kappa}{\tau_M}\left(\mathscr{D}_{3,1}(t) + \mathscr{D}_{3,2}(t)\right). \tag{28}
$$

By applying Lemma 1, it results in

$$
-\int_{-\tau_M}^{0} \Im(J_1, x(t+\theta))d\theta \le \frac{-1}{\tau_M}\Im\left(\mathscr{J}_1, \mathbf{D}\mathfrak{D}_1(t)\right) \tag{29}
$$

$$
-\int_{-\chi}^{0} \Im(J_2, x(t+\theta))d\theta \le \frac{-1}{\chi}\Im\left(\mathscr{J}_2, \mathfrak{D}_2(t)\right) \tag{30}
$$

$$
-\int_{-\eta_M}^{-\chi} \Im(J_3, x(t+\theta))d\theta \le \frac{-1}{\tau_M}\Im\left(\mathscr{J}_3, \mathbf{D}\mathfrak{D}_3(t)\right). \tag{31}
$$

From definition in (24) and (26)–(28), it results in

$$
\delta(t) = \Delta_1 \pi(t),\ \ \dot{\delta}(t) = \Delta_2 \pi(t). \tag{32}
$$

To guarantee the asymptotic stability of the closed-loop system (14), one needs

$$
\begin{aligned}
&\dot{V}(t) + \gamma^2 \omega^\top(t)\omega(t) - z^\top(t)z(t) \\
&\le 2\pi^\top(t)\Delta_1^{\top G}\Delta_2\pi(t) - \gamma^2\varpi^\top(t)\varpi(t) + z^\top(t)z(t) \\
&\quad + \Im(H_1 + \tau_M J_1 + H_2 + \chi J_2, \mathbf{e}_2\pi(t)) \\
&\quad - \Im(H_1, \mathbf{e}_3\pi(t)) + \Im(H_3 + \tau_M J_3 - H_2, \mathbf{e}_4\pi(t)) \\
&\quad - \Im(H_3, \mathbf{e}_5\pi(t)) - \frac{1}{\chi}\Im\left(\mathscr{J}_2, \mathbf{e}_b\pi(t)\right) \\
&\quad - \frac{1}{\tau_M}\Im\left(\mathscr{J}_1, \mathbf{D}\mathbf{e}_a\pi(t)\right) - \frac{1}{\tau_M}\Im\left(\mathscr{J}_3, \mathbf{D}\mathbf{e}_c\pi(t)\right) < 0.
\end{aligned} \tag{33}
$$

From (8) and (12), we have

$$
\rho_1\Im\left(\Omega, \left(\frac{C\Im}{\chi}\mathbf{e}_\chi - \mathbf{e}_{11+5\kappa}\right)\pi(t)\right) - \Im(\Omega, \mathbf{e}_{11+5\kappa}\pi(t)) > 0 \tag{34}
$$

$$
\Im(\Omega, \mathbf{e}_{11+5\kappa}\pi(t)) - \rho_2\Im\left(\Omega, \left(\frac{C\Im}{\chi}\mathbf{e}_\chi - \mathbf{e}_{11+5\kappa}\right)\pi(t)\right) > 0. \tag{35}
$$

By combining (29)–(35), it yields

$$
\begin{aligned}
&\dot{L}(t) + \gamma^2\omega^\top(t)\omega(t) - z^\top(t)z(t) \\
&\quad + a_1\left[\rho_1\Im\left(\Omega, \left(\frac{C\Im}{\chi}\mathbf{e}_\chi - \mathbf{e}_{11+5\kappa}\right)\pi(t)\right) - \Im(\Omega, \mathbf{e}_{11+5\kappa}\pi(t))\right] \\
&\quad + a_2\left[\Im(\Omega, \mathbf{e}_{11+5\kappa}\pi(t)) - \rho_2\Im\left(\Omega, \left(\frac{C\Im}{\chi}\mathbf{e}_\chi - \mathbf{e}_{11+5\kappa}\right)\pi(t)\right)\right] \\
&\le \Im(\Theta, \pi(t)) < 0
\end{aligned} \tag{36}
$$

where a_1 and a_2 are two positive scalars.

In terms of the definition of $\pi(t)$, the system (6) can be reformed as

$$
\sum_{i=1}^{2} \lambda_i \lambda_j^k \mathbf{Q}_{ij}\pi(t) = 0 \tag{37}
$$

where $\mathbf{Q}_{ij} = -I\mathbf{e}_1 + A_i\mathbf{e}_2 - BK_{1j}\mathbf{e}_\varepsilon + F\mathbf{e}_\varpi + (BK_j C\Im/\chi)(\mathbf{e}_b + \mathbf{e}_{a,1} - \mathbf{e}_{c,1})$ and $\Im = \left[I_n \quad 0_{n,\kappa n}\right]$.

By constructing $\mathbf{W} = \mu_1 \mathbf{e}_1^\top W + \mu_2 \mathbf{e}_2^\top W$, it yields

$$\sum_{i=1}^{2}\sum_{i=1}^{2}\lambda_i\lambda_j^k \Im\left(\mathbf{W}\mathbf{Q}_{ij}, \pi(t)\right) = 0. \tag{38}$$

In terms of the description of system (14), we have

$$\sum_{i=1}^{2}\sum_{i=1}^{2}\lambda_i\lambda_j^k \Im\left(\Pi_{ij}, \pi(t)\right) < 0. \tag{39}$$

Based on the property of fuzzy membership that $\sum_{i=1}^{2}\lambda_j = \sum_{i=1}^{2}\lambda_j^k = 1$, it yields

$$\sum_{i=1}^{2}\sum_{j=1}^{2}\lambda_i\left(\lambda_j - \lambda_j^k\right)\Im(\mho_i, \pi(t)) = 0. \tag{40}$$

Then, one deduces

$$\begin{aligned}\sum_{i=1}^{2}\sum_{j=1}^{2}\lambda_i\lambda_j^k\Im\left(\Pi_{ij}, \pi(t)\right) &= \sum_{i=1}^{2}\sum_{j=1}^{2}\lambda_i\lambda_j^k\Im\left(\Pi_{ij}, \pi(t)\right) \\ &\quad + \sum_{i=1}^{2}\sum_{j=1}^{2}\lambda_i\left(\lambda_j - \lambda_j^k\right)\Im\left(\mho_i, \pi(t)\right) \\ &= \sum_{i=1}^{2}\sum_{j=1}^{2}\lambda_i\lambda_j^k\Im\left(\Pi_{ij} - \mho_i, \pi(t)\right) + \sum_{i=1}^{2}\sum_{j=1}^{2}\lambda_i\lambda_j\Im\left(\mho_i, \pi(t)\right).\end{aligned} \tag{41}$$

According to $\lambda_j^k - \nu_j\lambda_j \geq 0$ and (41), it leads to

$$\begin{aligned}&\sum_{i=1}^{2}\sum_{j=1}^{2}\lambda_i\lambda_j^k\Im\left(\Pi_{ij}, \pi(t)\right) \\ &\leq \sum_{i=1}^{2}\sum_{j=1}^{2}\lambda_i\lambda_j\varsigma^\top(t)\Im\left(\nu_j\left(\Pi_{ij} - \mho_i\right), \pi(t)\right) \\ &\quad + \sum_{i=1}^{2}\sum_{j=1}^{2}\lambda_i\lambda_j\Im\left(\mho_i, \pi(t)\right) \\ &\leq \sum_{i=1}^{q}\sum_{j=1}^{q}\lambda_i\lambda_j\Im\left(\nu_i\left(\Pi_{ij} - \mho_i\right) + \mho_i, \pi(t)\right) \\ &\quad + \sum_{i=1}^{2}\sum_{i<j}\lambda_i\lambda_j\Im\left(\nu_j\left(\Pi_{ij} - \mho_i\right) + \mho_i\right. \\ &\quad \left. + \nu_i\left(\left(\Pi_{ij} - \mho_j\right)\right) + \mho_j, \pi(t)\right) < 0\end{aligned} \tag{42}$$

holds based on (17)–(19). ■

Remark 6: With the utilization of historical system information and considering the time-varying transmission delay, the time-varying distributed delay term $\int_{t-\tau(t)-\chi}^{t-\tau(t)} x(s)ds$ in (10) is introduced for system modeling and stability analysis, and it is difficult to be handled effectively by the existing method. Specifically, the conventional Simpson's rule in [37] and [38] to deal with it may lead to approximation error and conservativeness. To solve such difficulty, a new LKF (20) and an integral inequality in Lemma 1 both involved the distributed delay terms are used, which can remove the approximation error and lead to less conservative results.

Second, based on the results in the above theorem, the controller design conditions are obtained in Theorem 2.

Theorem 2: For given parameters $\bar{\tau}$, μ_i, a_i, ν_i, $(i = 1, 2)$, under the SMETM (8) with the scalars ρ_1, ρ_2, h, χ, the asymptotically stability with H_∞ norm bound γ of system (14) is ensured, if there exist symmetric matrices $\hat{G}$, $\hat{H}_b > 0$, $\hat{J}_b > 0$, $(b = 1, 2, 3)$, $\hat{\mathcal{J}}_r = \begin{bmatrix}\hat{J}_r & \hat{R}_r^\top \\ \hat{R}_r & \hat{J}_r\end{bmatrix} > 0$, $(r = 1, 3)$, $\hat{\Omega} > 0$ and matrices R and N_j such that

$$\hat{\mathscr{G}} > 0 \tag{43}$$
$$\hat{\Pi}_{ij} - \hat{\mho}_i < 0 \tag{44}$$
$$\hat{\digamma}_{ii} < 0 \tag{45}$$
$$\hat{\digamma}_{ij} + \hat{\digamma}_{ji} < 0, \quad (i < j) \tag{46}$$
$$\begin{bmatrix} -\epsilon I & * \\ (CR - YC) & -I \end{bmatrix} < 0 \tag{47}$$

where

$$\begin{aligned}\hat{\mathscr{G}} &= \hat{G} + \mathrm{diag}\left\{0, \hat{\mathscr{H}}_1, \hat{\mathscr{H}}_2, \hat{\mathscr{H}}_3\right\} \\ \hat{\mathscr{H}}_1 &= \mathfrak{R} \otimes \hat{H}_1, \hat{\mathscr{H}}_2 = \mathfrak{R} \otimes \hat{H}_2, \hat{\mathscr{H}}_3 = \mathfrak{R} \otimes \hat{H}_3 \\ \hat{\Pi}_{ij} &= \hat{\Theta} + He\left(\hat{\mathbf{W}}\hat{\mathbf{Q}}_{ij}\right),\ \hat{\digamma}_{ij} = \nu_j\left(\hat{\Pi}_{ij} - \hat{\mho}_i\right) + \hat{\mho}_i \\ \hat{\Theta} &= He\left(\Delta_1^\top \hat{G}\Delta_2\right) + \Im\left(\hat{H}_1 + \tau_M\hat{J}_1 + \hat{H}_2 + \chi\hat{J}_2, \mathbf{e}_2\right) \\ &\quad - \Im\left(\hat{H}_1, \mathbf{e}_3\right) + \Im\left(\hat{H}_3 + \tau_M\hat{J}_3 - \hat{H}_2, \mathbf{e}_4\right) - \Im\left(\hat{H}_3, \mathbf{e}_5\right) \\ &\quad - \frac{1}{\chi}\Im(\hat{\mathscr{J}}_2, \mathbf{e}_b) - \frac{1}{\tau_M}\Im(\hat{\mathscr{J}}_1, \mathbf{De}_a) - \frac{1}{\tau_M}\Im(\hat{\mathscr{J}}_3, \mathbf{De}_c) \\ &\quad + a_1\rho_1\Im\left(\hat{\Omega}, \frac{C\mathfrak{I}}{\chi}\mathbf{e}_\chi - \mathbf{e}_{11+5\kappa}\right) - a_1\Im\left(\hat{\Omega}, \mathbf{e}_{11+5\kappa}\right) \\ &\quad - a_2\rho_2\Im\left(\hat{\Omega}, \frac{C\mathfrak{I}}{\chi}\mathbf{e}_\chi - \mathbf{e}_{11+5\kappa}\right) + a_2\Im\left(\hat{\Omega}, \mathbf{e}_{11+5\kappa}\right) \\ &\quad - \gamma^2\Im(I, \mathbf{e}_{12+5\kappa}) - \Im(I, \mathbb{I}_{13+5\kappa}) + He\left(\mathbf{e}_{13+5\kappa}^\top CR\mathbf{e}_2\right) \\ \hat{\mathscr{J}}_2 &= \mathfrak{R} \otimes \hat{J}_2,\ \hat{\mathscr{J}}_1 = \hat{\mathcal{J}}_1 \otimes \mathfrak{R},\ \hat{\mathscr{J}}_3 = \hat{\mathcal{J}}_3 \otimes \mathfrak{R} \\ \hat{\mathbf{W}} &= \mu_1\mathbf{e}_1^\top + \mu_2\mathbf{e}_2^\top \\ \hat{\mathbf{Q}}_{ij} &= -R\mathbf{e}_1 + A_iR\mathbf{e}_2 - BN_j\mathbf{e}_{11+5\kappa} + F\mathbf{e}_{12+5\kappa} + \frac{BN_jC\mathfrak{I}}{\chi}\mathbf{e}_\chi.\end{aligned}$$

Thereby, the controller gain can be calculated from $K_j = N_jY^{-1}$.

Proof: Define $R = W^{-1}$, $\hat{\mathfrak{R}}_i = \Im(\mathfrak{R}_i, I_{n(5\kappa+11)} \otimes R)$, $\hat{H}_i = \Im(H_i, R)$, $\hat{J}_i = \Im(J_i, R)$, $i = 1, 2, 3$, $\hat{\mathscr{J}}_1 = \Im(\mathscr{J}_1, I_{n(2\kappa+2)} \otimes R)$, $\hat{\mathscr{J}}_2 = \Im(\mathscr{J}_2, I_{n(\kappa+1)} \otimes R)$, $\hat{\mathscr{J}}_3 = \Im(\mathscr{J}_3, I_{n(2\kappa+2)} \otimes R)$, $\hat{\Omega} = \Im(\Omega, Y)$.

Left- and right-multiplying (17) with $\mathscr{R}^\top = \mathrm{diag}\{R, R, R, R, R, I_{n(5(\kappa+1))} \otimes R, Y, I, I\}^\top$ and its transpose $\mathscr{R}$, we get

$$\bar{\Pi}_{ij} - \hat{\mho}_i < 0 \tag{48}$$

where

$$\begin{aligned}\bar{\Pi}_{ij} &= \bar{\Theta} + He\left(\hat{\mathbf{W}}\hat{\mathbf{Q}}_{ij}\right),\ \hat{\mho}_i = \Im\left(\mho_i, \mathscr{R}\right) \\ \bar{\Theta} &= He\left(\Delta_1^\top \hat{G}\Delta_2\right) + \Im\left(\hat{H}_1 + \tau_M\hat{J}_1 + \hat{H}_2 + \chi\hat{J}_2, \mathbf{e}_2\right) \\ &\quad - \Im\left(\hat{H}_1, \mathbf{e}_3\right) + \Im\left(\hat{H}_3 + \tau_M\hat{J}_3 - \hat{H}_2, \mathbf{e}_4\right) - \Im\left(\hat{H}_3, \mathbf{e}_5\right)\end{aligned}$$

TABLE I
SYSTEM PARAMETERS

Symbol	Value	Symbol	Value	Symbol	Value
$T_f(pu/Hz)$	0.015	$\varrho(Kg/m^3)$	1.225	$\mathbb{L}_m(pu)$	52
$M(pus)$	0.1667	$\mathbf{R}(m)$	5	$\mathbb{L}_s(pu)$	0.07397
$T_g(s)$	0.08	$\alpha(^\circ)$	0	$\mathbb{L}_r(pu)$	0.002
$T_t(s)$	0.4	$\beta_{opt}(pu)$	8.1	$w_s(m/s)$	1
$R_g(Hz/pu)$	3	$B_w(pu)$	150	$\mathbb{R}_s(pu)$	7.9
$\phi(pu)$	0.3483	$H_t(s)$	0.1	$\mathbb{R}_r(pu)$	2
$W_{rmax}(m/s)$	1.8	$W_{rmin}(m/s)$	-1.8		

$$
\begin{aligned}
&-\frac{1}{\chi}\Im\left(\hat{\mathscr{J}}_2, \mathbf{e}_b\right) - \frac{1}{\tau_M}\Im\left(\hat{\mathscr{J}}_1, \mathbf{De}_a\right) - \frac{1}{\tau_M}\Im\left(\hat{\mathscr{J}}_3, \mathbf{De}_c\right)\\
&+ a_1\rho_1\Im\left(\Omega, \frac{CR\Im}{\chi}\mathbf{e}_\chi - \mathbf{e}_{11+5\kappa}\right) - a_1\Im\left(\hat{\Omega}, \mathbf{e}_{11+5\kappa}\right)\\
&- a_2\rho_2\Im\left(\Omega, \frac{CR\Im}{\chi}\mathbf{e}_\chi - \mathbf{e}_{11+5\kappa}\right) + a_2\Im\left(\hat{\Omega}, \mathbf{e}_{11+5\kappa}\right)\\
&- \gamma^2\Im(I, \mathbf{e}_{12+5\kappa}) - \Im(I, \mathbb{I}_{13+5\kappa}) + He\left(\mathbf{e}_{13+5\kappa}^\top CR\mathbf{e}_2\right).
\end{aligned}
$$

According to the equality $CR = YC$ and defining $N_j = K_jY$, (48) equals to (44).

It is infeasible to solve the equation $CR = YC$ since it is not a strict inequality. Then, the problem of handling the nonlinear item BK_jCR in Theorem 1 can be converted as a *W-problem*. Based on $CR = YC$, it results in

$$(CR - YC)^\top(CR - YC) = 0. \tag{49}$$

By applying the Schur complement to (49), it yields

$$\begin{bmatrix} -\epsilon I & * \\ CR - YC & -I \end{bmatrix} < 0 \tag{50}$$

which is equivalent to (47) with a sufficient small scalar $\epsilon > 0$.

By taking the similar way to obtain (44), the conditions (45) and (46) are derived easily, which completes the proof. ■

Remark 7: The computational complexity of the controller design conditions in Theorem 2 mainly depends on the number of decision variables ($NoV = [(1 + (3\kappa + 4)n)(3\kappa + 4)n]/2$) in Lyapunov variable G, in which κ represents the degree of the vector $\mathcal{D}_{m,\kappa}$, $m = 1, 2, 3$, n means the amount of the state variables. With the increasement of κ, computational complexity is growing. Nevertheless, less conservative results could be obtained at the cost of more computational complexity.

IV. EXAMPLE

In this section, the values of parameters of WPS are given in Table I.

The external disturbance is considered as $\omega(t) = 0.2\sin(2t)$ for $t \in [0,\ 4\text{ s}]$ (otherwise, $w(t) = 0$).

The measurement outliers are characterized by a stochastic variable with bound 20 and emerge each 4 s starting from $t = 1$ s, which are shown in Fig. 2.

Choose the other parameters as $\chi = 0.1$, $h = 0.01$, $\bar{\tau} = 0.08$, $\tau_M = \bar{\tau} + h = 0.09$, $\rho_1 = 0.02$, $\rho_2 = 10$, $\mu_1 = 5$, $\mu_2 = 50$, $a_1 = 10$, $a_2 = 1$, $\epsilon = 0.01$, and $\nu_1 = \nu_2 = 0.9$. By solving the conditions in Theorem 2, the optimized H_∞ index is obtained as $\gamma = 1.5523$, and the fuzzy controller gains and triggering matrix are derived as

$$K_1 = \begin{bmatrix} 0.7066 & -0.1825 & -2.1470 & 0.0479 \end{bmatrix}$$

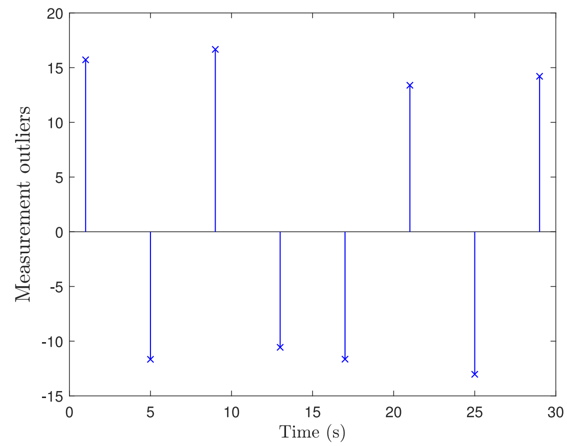

Fig. 2. Measurement outliers with bound 20.

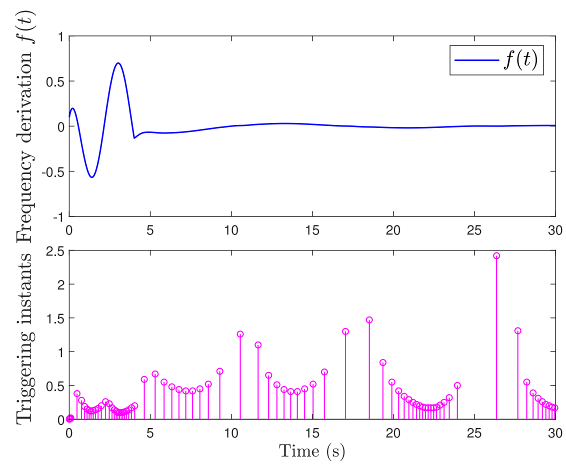

Fig. 3. Frequency derivation and triggering instants.

$$K_2 = \begin{bmatrix} 0.8312 & -0.1720 & 2.3789 & -0.0433 \end{bmatrix}$$

$$\Omega = \begin{bmatrix} 7.1046 & 2.8457 & 4.8628 & 0.0436 \\ 2.8457 & 79.2370 & 1.3261 & 0.0294 \\ 4.8628 & 1.3261 & 224.4186 & -4.3973 \\ 0.0436 & 0.0294 & -4.3973 & 0.3920 \end{bmatrix}.$$

In the simulation, for the initial condition $x(0) = [0.1, -0.2, 0.2, 0, 0.1, -0.2]^\top$, the frequency deviation of WPS and the triggering instants are shown in Fig. 3. In terms of this figure, the designed event-triggered fuzzy controller is effective to ensure the frequency stable when the measurement outliers and transmission delays occur.

Next, two comparison cases are carried out to further illustrate the merits of the investigated SMETM over some existing ETMs.

A. First Comparison Case

This case shows that the proposed SMETM is more effective in decreasing the redundant triggering events than ORETM in [36] without considering memory system information.

The external disturbance is considered as $\omega(t) = \psi(t)e^{-0.2t}$ for $t \geq 5.5$ s and $\omega(t) = 0$ for $t < 5.5$ s, in which $\psi(t) \in [-3,\ 3]$ is a stochastic variable.

Considering the measurement outliers, the obtained controller gains, and triggering matrix in the above simulation,

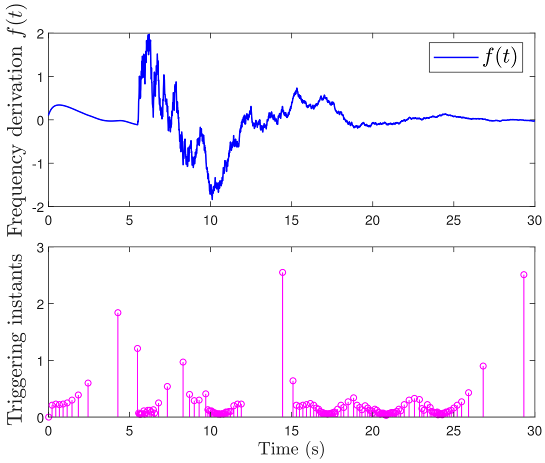

Fig. 4. Frequency derivation and triggering instants under ORETM [36].

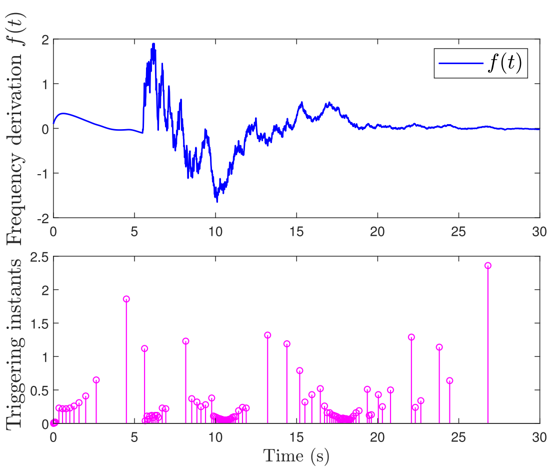

Fig. 5. Frequency derivation and triggering instants under SMETM for the first comparison case.

TABLE II
AMOUNT OF EVENTS $\Re$ UNDER THE DIFFERENT ETMs FOR THE FIRST COMPARISON CASE

Method	$\Re$
ORETM [36]	145
Our SMETM (8)	101

the curves of frequency deviation and the triggering times obtained by existing ORETM and our SMETM are drawn in Figs. 4 and 5. Meanwhile, Table II compares that the number ($\Re$) of triggering events generated by the existing ORETM and our SMETM. According to Figs. 4 and 5, one observes the trajectories of $f(t)$ generated by the two ETMs are very similar. However, Table II tells that $\Re$ obtained by our SMETM (8) is significantly reduced 30.3% compared to the existing ORETM [36], which verifies the effectiveness of SMETM for lowering the triggering rate.

B. Second Comparison Case

To demonstrate the merit of the presented SMETM to exclude the false triggering events caused by measurement outliers, the following comparisons between SMETM and normal ETM [23] are executed. The disturbance is the same with

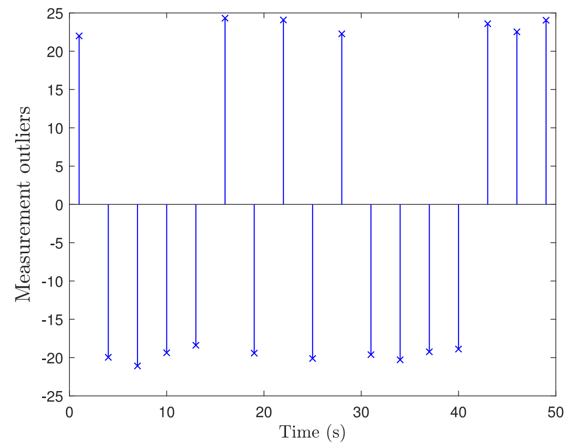

Fig. 6. Measurement outliers with bound 25.

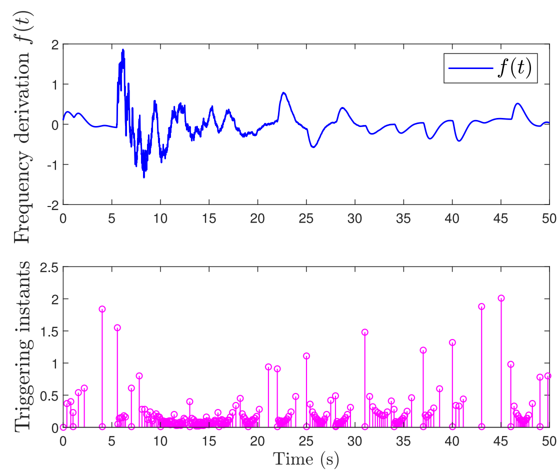

Fig. 7. Frequency derivation and triggering instants under normal ETM.

the first case. The measurement outliers are featured by a stochastic variable bound 25 and emerge each 3 s starting from $t = 1$ s, which are shown in Fig. 6.

In this case, we choose $\chi = 0.06$ and $\rho_1 = 0.05$, the other parameters are the same with the above case. Then, solving Theorem 2, one obtains $\gamma = 1.6185$ and

$$K_1 = \begin{bmatrix} 0.2593 & -0.1389 & -1.6165 & 0.0423 \end{bmatrix}$$
$$K_2 = \begin{bmatrix} 0.3561 & -0.1287 & 1.7104 & -0.0417 \end{bmatrix}$$
$$\Omega = \begin{bmatrix} 5.1525 & 1.3626 & 3.5987 & 0.0467 \\ 1.3626 & 54.1728 & 1.3215 & 0.0026 \\ 3.5987 & 1.3215 & 156.8844 & -3.7944 \\ 0.0467 & 0.0026 & -3.7944 & 0.4726 \end{bmatrix}.$$

By using the derived parameters, the responses of frequency deviation and the triggering instants under two different ETMs are drawn in Figs. 7 and 8, respectively. The number $\Re$ produced by normal ETM and our SMETM is given in Table III. It is observed from Fig. 7 that the stability of frequency is degraded obviously by outliers under the normal ETM. However, by discarding the undesired triggering events resulted from outliers, the frequency obtained by our SMETM is more stable. Additionally, the triggering events are also decreased dramatically by using our SMETM than the normal ETM.

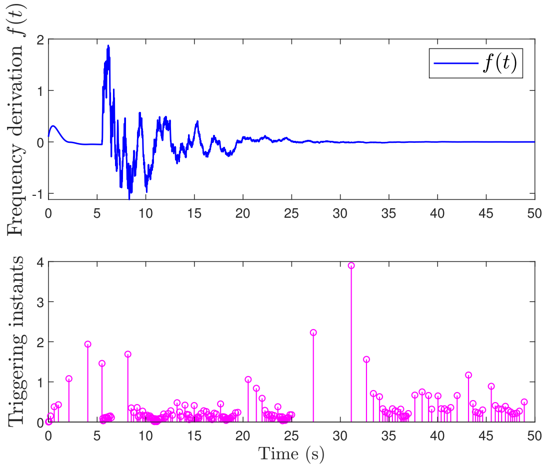

Fig. 8. Frequency derivation and triggering instants under SMETM for the second comparison case.

TABLE III
AMOUNT OF EVENTS $\mathfrak{N}$ UNDER THE DIFFERENT ETMs FOR THE SECOND COMPARISON CASE

Method	$\mathcal{N}$
Normal ETM [23]	258
Our SMETM	186

V. CONCLUSION

This article has addressed the event-triggered LFC problem of T–S fuzzy WPSs against outliers and transmission delays. A new SMETM using the system memory outputs is constructed to reduce the unnecessary transmissions induced by external disturbances. Moreover, to exclude the negative effect from measurement outliers, the triggering error signal is further required to be less than an upper bound. Then, the closed-loop system is modeled as a T–S fuzzy system with time-varying distributed delay. Some sufficient LMI conditions are accomplished to solve the fuzzy controller gains and the triggering matrix. Finally, some simulations are implemented to illustrate the merits of the presented method. Note that a time-varying weighting function is more general than the considered SMETM with the same weight for the historical signals. Thus, how to design the memory-event-triggered controller under the time-varying weighting function case deserves further investigations in our future work.

REFERENCES

[1] P. Mani, J. H. Lee, K. W. Kang, and Y. H. Joo, "Digital controller design via LMIs for direct-driven surface mounted PMSG-based wind energy conversion system," *IEEE Trans. Cybern.*, vol. 50, no. 7, pp. 3056–3067, Jul. 2020.

[2] L. Jin, Y. He, C.-K. Zhang, X.-C. Shangguan, L. Jiang, and M. Wu, "Robust delay-dependent load frequency control of wind power system based on a novel reconstructed model," *IEEE Trans. Cybern.*, vol. 52, no. 8, pp. 7825–7836, Aug. 2022, doi: 10.1109/TCYB.2021.3051160.

[3] C. N. Mukundan, S. B. Q. Naqvi, Y. Singh, B. Singh, and P. Jayaprakash, "A cascaded generalized integral control for multiobjective grid-connected solar energy transfer system," *IEEE Trans. Ind. Electron.*, vol. 68, no. 12, pp. 12385–12395, Dec. 2021.

[4] J. Liu et al., "Impact of power grid strength and PLL parameters on stability of grid-connected DFIG wind farm," *IEEE Trans. Sustain. Energy*, vol. 11, no. 1, pp. 545–557, Jan. 2020.

[5] L. Shanmugam and Y. H. Joo, "Stability and stabilization for T–S fuzzy large-scale interconnected power system with wind farm via sampled-data control," *IEEE Trans. Syst., Man, Cybern., Syst.*, vol. 51, no. 4, pp. 2134–2144, Apr. 2020.

[6] P. Buduma, N. K. Vulisi, and G. Panda, "Robust control and Kalman MPPT for grid-assimilated wind energy conversion system," *IEEE Trans. Ind. Appl.*, vol. 57, no. 2, pp. 1274–1284, Mar./Apr. 2021.

[7] Z. Lian, P. Shi, C.-C. Lim, and X. Yuan, "Fuzzy-model-based lateral control for networked autonomous vehicle systems under hybrid cyber-attacks," *IEEE Trans. Cybern.*, early access, Mar. 14, 2022, doi: 10.1109/TCYB.2022.3151880.

[8] Z. Lian, P. Shi, and C. C. Lim, "Dynamic hybrid-triggered-based fuzzy control for nonlinear networks under multiple cyber-attacks," *IEEE Trans. Fuzzy Syst.*, vol. 30, no. 9, pp. 3940–3951, Sep. 2022.

[9] X. Xie, C. Wei, Z. Gu, and K. Shi, "Relaxed resilient fuzzy stabilization of discrete-time Takagi–Sugeno systems via a higher order time-variant balanced matrix method," *IEEE Trans. Fuzzy Syst.*, vol. 30, no. 11, pp. 5044–5050, Nov. 2022, doi: 10.1109/TFUZZ.2022.3145809.

[10] Z. Gu, D. Yue, J. H. Park, and X. Xie, "Memory-event-triggered fault detection of networked IT2 TS fuzzy systems," *IEEE Trans. Cybern.*, early access, Mar. 14, 2022, doi: 10.1109/TCYB.2022.3155755.

[11] Y. Li, T. Wang, W. Liu, and S. Tong, "Neural network adaptive output-feedback optimal control for active suspension systems," *IEEE Trans. Syst., Man, Cybern., Syst.*, vol. 52, no. 6, pp. 4021–4032, Jun. 2022.

[12] Y. Li, J. Zhang, W. Liu, and S. Tong, "Observer-based adaptive optimized control for stochastic nonlinear systems with input and state constraints," *IEEE Trans. Neural Netw. Learn. Syst.*, early access, Jun. 23, 2021, doi: 10.1109/TNNLS.2021.3087796.

[13] S. Ghosh, S. Kamalasadan, N. Senroy, and J. Enslin, "Doubly fed induction generator (DFIG)-based wind farm control framework for primary frequency and inertial response application," *IEEE Trans. Power Syst.*, vol. 31, no. 3, pp. 1861–1871, May 2016.

[14] R. Venkateswaran and Y. H. Joo, "Retarded sampled-data control design for interconnected power system with DFIG-based wind farm: LMI approach," *IEEE Trans. Cybern.* vol. 52, no. 7, pp. 5767–5777, Jul. 2022, doi: 10.1109/TCYB.2020.3042543.

[15] H. Zeng, S. Zhou, X. Zhang, and W. Wang, "Delay-dependent stability analysis of load frequency control systems with electric vehicles," *IEEE Trans. Cybern.*, vol. 52, no. 12, pp. 13645–13653, Dec. 2022, doi: 10.1109/TCYB.2022.3140463.

[16] Z. Hu, S. Liu, W. Luo, and L. Wu, "Resilient distributed fuzzy load frequency regulation for power systems under cross-layer random denial-of-service attacks," *IEEE Trans. Cybern.*, vol. 52, no. 4, pp. 2396–2406, Apr. 2022.

[17] Z. Yan and Y. Xu, "A multi-agent deep reinforcement learning method for cooperative load frequency control of a multi-area power system," *IEEE Trans. Power Syst.*, vol. 35, no. 6, pp. 4599–4608, Nov. 2020.

[18] Z. Gu, D. Yue, C. K. Ahn, S. Yan, and X. Xie, "Segment-weighted information-based event-triggered mechanism for networked control systems,"*IEEE Trans. Cybern.*, early access, Oct. 27, 2022, doi: 10.1109/TCYB.2022.3215015.

[19] F. Yang, J. He, and Q. Pan, "Further improvement on delay-dependent load frequency control of power systems via truncated B–L inequality," *IEEE Trans. Power Syst.*, vol. 33, no. 5, pp. 5062–5071, Sep. 2018.

[20] S. Yan, Z. Gu, J. H. Park, X. Xie, and C. Dou, "Probability-density-dependent load frequency control of power systems with random delays and cyber-attacks via circuital implementation," *IEEE Trans. Smart Grid*, vol. 13, no. 6, pp. 4837–4847, Nov. 2022.

[21] J. P. Farwell and R. Rohozinski, "Stuxnet and the future of cyber war," *Survival*, vol. 53, no. 1, pp. 23–40, 2011.

[22] L. Jiang, W. Yao, Q. H. Wu, J. Y. Wen, and S. J. Cheng, "Delay-dependent stability for load frequency control with constant and time-varying delays," *IEEE Trans. Power Syst.*, vol. 27, no. 2, pp. 932–941, May 2012.

[23] X.-M. Zhang and Q.-L. Han, "Event-based H_∞ filtering for sampled-data systems," *Automatica*, vol. 51, pp. 55–69, Jan. 2015.

[24] P. Shi, H. Wang, and C.-C. Lim, "Network-based event-triggered control for singular systems with quantizations," *IEEE Trans. Ind. Electron.*, vol. 63, no. 2, pp. 1230–1238, Feb. 2016.

[25] X. Su, C. Wang, H. Chang, Y. Yang, and W. Assawinchaichote, "Event-triggered sliding mode control of networked control systems with Markovian jump parameters," *Automatica*, vol. 125, Mar. 2021, Art. no. 109405.

[26] X. Sun, Z. Gu, D. Yue, and X. Xie, "Event-triggered H_∞filtering for cyber–physical systems against DoS attacks,"*IEEE Trans. Syst., Man, Cybern., Syst.*, early access, Nov. 8, 2022, doi: 10.1109/TSMC.2022.3218023.

[27] X. Yin, Z. Gao, D. Yue, and S. Hu, "Cloud-based event-triggered predictive control for heterogeneous NMASs under both DoS attacks and transmission delays," *IEEE Trans. Syst., Man, Cybern., Syst.*, vol. 52, no. 12, pp. 7482–7493, Dec. 2022.

[28] L. Ding, Q. L. Han, and X.-M. Zhang, "Distributed secondary control for active power sharing and frequency regulation in islanded microgrids using an event-triggered communication mechanism," *IEEE Trans. Ind. Informat.*, vol. 15, no. 7, pp. 3910–3922, Jul. 2019.

[29] H. Zhang, J. Liu, and S. Xu, "H_∞ load frequency control of networked power systems via an event-triggered scheme," *IEEE Trans. Ind. Electron.*, vol. 67, no. 8, pp. 7104–7113, Aug. 2020.

[30] S. Saxena and E. Fridman, "Event-triggered load frequency control via switching approach," *IEEE Trans. Power Syst.*, vol. 35, no. 6, pp. 4484–4494, Nov. 2020.

[31] E. Tian and C. Peng, "Memory-based event-triggering H_∞ load frequency control for power systems under deception attacks," *IEEE Trans. Cybern.*, vol. 50, no. 11, pp. 4610–4618, Nov. 2020.

[32] J. Yang, Q. Zhong, K. Shi, and S. Zhong, "Co-design of observer-based fault detection filter and dynamic event-triggered controller for wind power system under dual alterable DoS attacks," *IEEE Trans. Inf. Forensics Security*, vol. 17, pp. 1270–1284, 2022.

[33] G. Liu, J. H. Park, C. Hua, and Y. Li, "Hybrid dynamic event-triggered load frequency control for power systems with unreliable transmission networks," *IEEE Trans. Cybern.*, early access, Apr. 12, 2022, doi: 10.1109/TCYB.2022.3163271.

[34] J. Li, Z. Wang, H. Dong, and G. Ghinea, "Outlier-resistant remote state estimation for recurrent neural networks with mixed time-delays," *IEEE Trans. Neural Netw. Learn. Syst.*, vol. 32, no. 5, pp. 2266–2273, May 2021.

[35] Z. Zhang and J. Dong, "Observer-based interval type-2 $L_2 - -L_\infty/H_\infty$ mixed fuzzy control for uncertain nonlinear systems under measurement outliers," *IEEE Trans. Syst., Man, Cybern., Syst.*, vol. 51, no. 12, pp. 7652–7662, Dec. 2021.

[36] X. Zhao, C. Liu, J. Liu, and E. Tian, "Probabilistic-constrained reliable H_∞ tracking control for a class of stochastic nonlinear systems: An outlier-resistant event-triggered scheme," *J. Franklin Inst.*, vol. 358, no. 9, pp. 4741–4760, 2021.

[37] S. H. Mousavi and H. J. Marquez, "Integral-based event triggering controller design for stochastic LTI systems via convex optimisation," *Int. J. Control*, vol. 89, no. 7, pp. 1416–1427, 2016.

[38] X. Wang, Z. Fei, H. Gao, and J. Yu, "Integral-based event-triggered fault detection filter design for unmanned surface vehicles," *IEEE Trans. Ind. Informat.*, vol. 15, no. 10, pp. 5626–5636, Oct. 2019.

[39] S. Saxena and Y. V. Hote, "Load frequency control in power systems via internal model control scheme and model-order reduction," *IEEE Trans. Power Syst.*, vol. 28, no. 3, pp. 2749–2757, Aug. 2013.

[40] S. Yan, Z. Gu, and J. H. Park, "Memory-event-triggered H_∞ load frequency control of multi-area power systems with cyber-attacks and communication delays," *IEEE Trans. Netw. Sci. Eng.*, vol. 8, no. 2, pp. 1571–1583, Apr.–Jun. 2021.

[41] P. Mani and Y. H. Joo, "Fuzzy logic-based integral sliding mode control of multi-area power systems integrated with wind farms," *Inf. Sci.*, vol. 545, pp. 153–169, Feb. 2021.

[42] C. Peng, M. Wu, X. Xie, and Y. L. Wang, "Event-triggered predictive control for networked nonlinear systems with imperfect premise matching," *IEEE Trans. Fuzzy Syst.*, vol. 26, no. 5, pp. 2797–2806, Oct. 2018.

[43] J. Liu, Y. Gu, L. Zha, Y. Liu, and J. Cao, "Event-triggered H_∞ load frequency control for multiarea power systems under hybrid cyber attacks," *IEEE Trans. Syst., Man, Cybern., Syst.*, vol. 49, no. 8, pp. 1665–1678, Aug. 2019.

[44] S. Yan, S. K. Nguang, and Z. Gu, "H_∞ weighted integral event-triggered synchronization of neural networks with mixed delays," *IEEE Trans. Ind. Informat.*, vol. 17, no. 4, pp. 2365–2375, Apr. 2021.

[45] A. Seuret and F. Gouaisbaut, "Stability of linear systems with time-varying delays using Bessel–Legendre inequalities," *IEEE Trans. Autom. Control*, vol. 63, no. 1, pp. 225–232, Jan. 2018.

[46] Q. Feng, S. K. Nguang, and W. Perruquetti, "Dissipative stabilization of linear systems with time-varying general distributed delays," *Automatica*, vol. 122, Dec. 2020, Art. no. 109227.

[47] N. J. Higham and M. Mikaitis, "Anymatrix: An extensible MATLAB matrix collection," *Numer. Algorithms*, vol. 90, no. 3, pp. 1175–1196, Jul. 2022.

[48] Q. Feng and S. K. Nguang, "Stabilization of uncertain linear distributed delay systems with dissipativity constraints," *Syst. Control Lett.*, vol. 96, pp. 60–71, Oct. 2016.

[49] C. Peng, J. Li, and M. Fei, "Resilient event-triggering H_∞ load frequency control for multi-area power systems with energy-limited DoS attacks,"*IEEE Trans. Power Syst.*, vol. 32, no. 5, pp. 4110–4118, Sep. 2017.

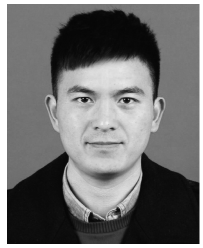

Shen Yan received the B.E. and Ph.D. degrees from the College of Electrical Engineering and Control Science, Nanjing Tech University, Nanjing, China, in 2014 and 2019, respectively.

From November 2017 to November 2018, he was a visiting Ph.D. student with the University of Auckland, Auckland, New Zealand. From February 2022 to August 2022, he was a Visiting Scholar with Yeungnam University, Gyeongsan, Republic of Korea. He is currently an Associate Professor with the College of Mechanical and Electronic Engineering, Nanjing Forestry University, Nanjing. His current research interests include networked control systems, event-triggered control, and their applications.

Zhou Gu (Member, IEEE) received the B.S. degree from North China Electric Power University, Beijing, China, in 1997, and the M.S. and Ph.D. degrees in control science and engineering from the Nanjing University of Aeronautics and Astronautics, Nanjing, China, in 2007 and 2010, respectively.

From September 1999 to January 2013, he was with the School of Power Engineering, Nanjing Normal University, Nanjing, as an Associate Professor. He was a Visiting Scholar with Central Queensland University, Rockhampton, QLD, Australia, and The University of Manchester, Manchester, U.K. He is currently a Professor with Nanjing Forestry University, Nanjing. His current research interests include networked control systems, time-delay systems, reliable control, and their applications.

Ju H. Park (Senior Member, IEEE) received the Ph.D. degree in electronics and electrical engineering from the Pohang University of Science and Technology (POSTECH), Pohang, Republic of Korea, in 1997.

From May 1997 to February 2000, he was a Research Associate with the Engineering Research Center-Automation Research Center, POSTECH. He joined Yeungnam University, Gyeongsan, Republic of Korea, in March 2000, where he is currently the Chuma Chair Professor. He is a coauthor of the monographs *Recent Advances in Control and Filtering of Dynamic Systems With Constrained Signals* (New York, NY, USA: Springer-Nature, 2018) and *Dynamic Systems With Time Delays: Stability and Control* (New York, NY, USA: Springer-Nature, 2019) and is an Editor of an edited volume *Recent Advances in Control Problems of Dynamical Systems and Networks* (New York, NY, USA: Springer-Nature, 2020). His research interests include robust control and filtering, neural/complex networks, fuzzy systems, multiagent systems, and chaotic systems. He has published a number of articles in the above areas.

Prof. Park has been a recipient of the Highly Cited Researchers Award by Clarivate Analytics (formerly, Thomson Reuters) since 2015, and listed in three fields, Engineering, Computer Sciences, and Mathematics, in 2019–2022. He also serves as an Editor for the *International Journal of Control, Automation and Systems*. He is also a Subject Editor/Advisory Editor/Associate Editor/Editorial Board Member of several international journals, including *IET Control Theory and Applications*, *Applied Mathematics and Computation*, *Journal of The Franklin Institute*, *Nonlinear Dynamics*, *Engineering Reports*, *Cogent Engineering*, the IEEE TRANSACTION ON FUZZY SYSTEMS, the IEEE TRANSACTION ON NEURAL NETWORKS AND LEARNING SYSTEMS, and the IEEE TRANSACTION ON CYBERNETICS. He is a Fellow of the Korean Academy of Science and Technology.

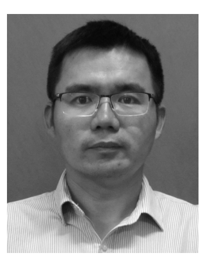

Xiangpeng Xie (Member, IEEE) received the B.S. and Ph.D. degrees in engineering from Northeastern University, Shenyang, China, in 2004 and 2010, respectively.

From 2010 to 2014, he was a Senior Engineer with Metallurgical Corporation of China Ltd., Beijing, China. He is currently a Professor with the Institute of Advanced Technology, Nanjing University of Posts and Telecommunications, Nanjing, China. His research interests include fuzzy modeling and control synthesis, state estimations, optimization in process industries, and intelligent optimization algorithms.

Prof. Xie serves as an Associate Editor for the *International Journal of Control, Automation, and Systems* and the *International Journal of Fuzzy Systems*.